

Anti-parity-time symmetry hidden in a damping linear resonator

Xun-Wei Xu,^{*} Jie-Qiao Liao,[†] Hui Jing,[‡] and Le-Man Kuang[§]

*Key Laboratory of Low-Dimensional Quantum Structures and Quantum Control of Ministry of Education,
Key Laboratory for Matter Microstructure and Function of Hunan Province,
Department of Physics and Synergetic Innovation Center for Quantum Effects and Applications,
Hunan Normal University, Changsha 410081, China*

(Dated: October 27, 2023)

Phase transition from the over-damping to under-damping states is a ubiquitous phenomenon in physical systems. However, what kind of symmetry is broken associated with this phase transition remains unclear. Here, we discover that this phase transition is determined by an anti-parity-time (anti- \mathcal{PT}) symmetry hidden in a single damping linear resonator, which is significantly different from the conventional anti- \mathcal{PT} -symmetric systems with two or more modes. We show that the breaking of the anti- \mathcal{PT} symmetry yields the phase transition from the over-damping to under-damping states, with an exceptional point (EP) corresponding to the critical-damping state. Moreover, we propose an optomechanical scheme to show this anti- \mathcal{PT} symmetry breaking by using the optical spring effect in a quadratic optomechanical system. We also suggest an optomechanical sensor with the sensitivity enhanced significantly around the EPs for the anti- \mathcal{PT} symmetry breaking. Our work unveils the anti- \mathcal{PT} symmetry hidden in damping oscillations and hence opens up new possibilities for exploiting wide anti- \mathcal{PT} symmetry applications in single damping linear resonators.

I. INTRODUCTION

Damping oscillation is one of the most fundamental and important physical processes [1], and such behavior appears in various physical systems, such as electronic, atomic, mechanical (acoustic), and optical (photonic) resonators. It is well known that a damping resonator undergoes a phase transition from the monotonically damping without oscillation (over-damping) to an oscillatory behavior with a damping amplitude (under-damping), crossing the critical condition that the damping rate is twice the value of the resonant frequency. However, there is no discussion on *whether there exists some kind of symmetry breaking determining this phase transition*. According to the quantum theory of open systems [2], the damping effect can be described simply with a damping term by eliminating the reservoir coupled to the resonator, and hence the symmetry in the damping oscillator should be discussed based on a non-Hermitian Hamiltonian including the damping term. In the past decades, the non-Hermitian physics with parity-time (\mathcal{PT}) symmetry [3–7] has attracted intense interest from photonics [8–23] to acoustics [24–28] and other communities [29–40]. However, a damping linear resonator does not satisfy the conditions of \mathcal{PT} symmetry for the requirement of a gain to balance the loss.

Anti- \mathcal{PT} symmetry [41] is another non-Hermitian symmetry attracted considerable theoretical and experimental interests [42–67]. The breaking of anti- \mathcal{PT} symmetry leads to exotic functionalities with pure dissipation,

such as unidirectional reflectionless [42, 43], chiral mode switching [44–46], and precision quantum sensing [49, 66]. A tremendous effort has also been devoted to achieving anti- \mathcal{PT} symmetry by using either dissipative coupling [50–64] or parametric (nonlinear) driving [46–48]. Nevertheless, the relation between the anti- \mathcal{PT} symmetry breaking and phase transition from the over-damping to under-damping states has not been revealed yet.

In this work, we find that *the dynamical Hamiltonian matrix of a damping linear resonator is anti- \mathcal{PT} symmetric*, and that the breaking of the anti- \mathcal{PT} symmetry induces the phase transition from the over-damping to under-damping states crossing the critical-damping state corresponding to an exceptional point (EP). Different from the conventional anti- \mathcal{PT} -symmetric systems that two or more modes are required [50–63], here the anti- \mathcal{PT} symmetry is found in a single-mode system, which greatly expands its range of applications. Moreover, we propose an optomechanical scheme [68] to observe this anti- \mathcal{PT} symmetry breaking for a damping mechanical resonator in a quadratic optomechanical system [69–81] based on the optical string effect [82–84]. We show that the breaking of the anti- \mathcal{PT} symmetry in a damping mechanical resonator can be used for ultra-sensitive sensing based on the frequency splitting around the EPs. The results presented in this work are general and hence these physics can be observed in other damping linear resonant platforms, including atomic [50–52], electrical [53], thermal [54], optical [55–60], magnonic [61, 62] and mechanical [63] systems.

II. ANTI- \mathcal{PT} SYMMETRY

We consider a damping linear resonator with mass M and spring constant k , which is described by a Hamil-

^{*} Corresponding author: xwxu@hunnu.edu.cn

[†] Corresponding author: jqiao@hunnu.edu.cn

[‡] Corresponding author: jinghui73@gmail.com

[§] Corresponding author: lmkuang@hunnu.edu.cn

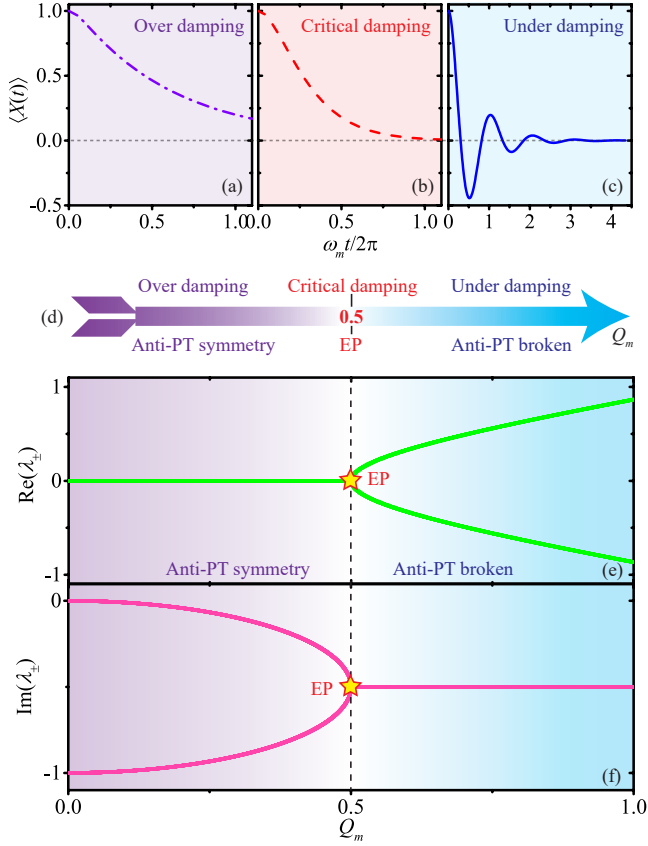


FIG. 1. (Color online) The dynamics of the mean value $\langle X \rangle \equiv \langle x \rangle / \sqrt{\hbar/(M\omega_m)}$ for three damping states: (a) over damping ($Q_m = 0.25$), (b) critical damping ($Q_m = 0.5$), and (c) under damping ($Q_m = 2$), under the initial conditions $\langle X(0) \rangle = 1$ and $\langle p(0) \rangle = 0$. (d) The correspondence between the dynamic states and the sorts of symmetry for a damping linear resonator. (e) Real and (f) imaginary parts of the eigenvalues λ_{\pm} of $H_{\text{dym}}/(\hbar\gamma_m)$ with an EP at $Q_m = 0.5$.

tonian $H_{\text{MR}} = p^2/(2M) + kx^2/2$ with the displacement x and momentum p , and $\omega_m = \sqrt{k/M}$ is the resonant frequency of the mechanical resonator. The equations of motion for the mean values $\langle x \rangle$ and $\langle p \rangle$ are given by $d\langle x \rangle/dt = \langle p \rangle/M$ and $d\langle p \rangle/dt = -k\langle x \rangle - \gamma_m\langle p \rangle$, where γ_m is the damping rate induced by the couplings to the thermal reservoir [85]. We already know that the damping mechanical resonator exhibits over-damping, critical-damping, and under-damping states, corresponding to $\omega_m < \gamma_m/2$, $\omega_m = \gamma_m/2$, and $\omega_m > \gamma_m/2$, as shown in Figures 1(a)-1(c). Although the phase transition for these dynamic behaviors is widely known, the associated intrinsic symmetry breaking has not been discovered yet.

Below we show that the dynamical Hamiltonian matrix of a damping mechanical resonator is anti- \mathcal{PT} symmetric, and the over-, under- and critical-damping states are associated with the phases of anti- \mathcal{PT} symmetry, anti- \mathcal{PT} broken, and EP, respectively. To reveal the anti- \mathcal{PT} symmetry in a damping mechanical resonator, we rewrite the mechanical displacement and momen-

tum as $x = x_{\text{zp}}(b^\dagger + b)$ and $p = ip_{\text{zp}}(b^\dagger - b)$, with $x_{\text{zp}} = \sqrt{\hbar/(2M\omega_m)}$, $p_{\text{zp}} = \sqrt{\hbar M\omega_m/2}$, and $[b, b^\dagger] = 1$. Then the equations of motion are rewritten as $id(\langle b \rangle, \langle b^\dagger \rangle)^T/dt = H_{\text{dym}}(\langle b \rangle, \langle b^\dagger \rangle)^T$ (“ T ” denoting matrix transpose), where the dynamical Hamiltonian matrix H_{dym} is given by

$$\frac{H_{\text{dym}}}{\hbar\gamma_m} = \begin{pmatrix} Q_m - i/2 & i/2 \\ i/2 & -Q_m - i/2 \end{pmatrix} \quad (1)$$

with the quality factor $Q_m \equiv \omega_m/\gamma_m$. The H_{dym} in Eq. (1) is anti- \mathcal{PT} -symmetric as

$$(\mathcal{PT})H_{\text{dym}}(\mathcal{PT})^{-1} = -H_{\text{dym}}, \quad (2)$$

with the parity operation \mathcal{P} for switching $b \leftrightarrow b^\dagger$ and the time-reversal operation \mathcal{T} for complex conjugation. The eigenvalues of $H_{\text{dym}}/(\hbar\gamma_m)$ are

$$\lambda_{\pm} = -i/2 \pm \sqrt{Q_m^2 - 1}/4, \quad (3)$$

corresponding to the eigenstates $\Psi_{\pm} = (\beta_{\pm}, \beta'_{\pm})^T$, with coefficients $\beta_{\pm}/\beta'_{\pm} = -i2Q_m \pm \sqrt{1 - 4Q_m^2}$. It should be mentioned that λ_{\pm} in Eq. (3) are also the eigenvalues of the dynamical Hamiltonian matrix for the mean values of the dimensionless position $X \equiv x/(\sqrt{2}x_{\text{zp}})$ and momentum $P \equiv p/(\sqrt{2}p_{\text{zp}})$, as $id(\langle X \rangle, \langle P \rangle)^T/dt = H'_{\text{dym}}(\langle X \rangle, \langle P \rangle)^T$, with

$$\frac{H'_{\text{dym}}}{\hbar\gamma_m} = \begin{pmatrix} 0 & iQ_m \\ -iQ_m & -i \end{pmatrix}. \quad (4)$$

So λ_{\pm} in Eq. (3) are physical and can be measured experimentally.

The phases for the damping mechanical resonator can be discovered by analyzing both the real and imaginary parts of the eigenvalues λ_{\pm} [Figures 1(e) and 1(f)]. We can see a phase transition from the anti- \mathcal{PT} -symmetric to the anti- \mathcal{PT} broken phases occurring at $Q_m = 0.5$. In the anti- \mathcal{PT} -symmetric phase with $Q_m < 0.5$, Ψ_{\pm} are also the eigenstates of the parity-time operator \mathcal{PT} , corresponding to the over-damping state. In the anti- \mathcal{PT} broken phase with $Q_m > 0.5$, Ψ_{\pm} are no longer the eigenstates of the parity-time operator \mathcal{PT} , corresponding to the under-damping state. Moreover, the critical point $Q_m = 0.5$ for the anti- \mathcal{PT} phase transition, namely EP, corresponds to the critical-damping state. The correspondence between the dynamic states and the sorts of symmetry for a damping mechanical resonator is shown in Figure 1(d). As the symmetry of the damping resonator depends on the value of Q_m , the anti- \mathcal{PT} symmetry breaking can be realized by adjusting either the decay rate γ_m or the resonant frequency ω_m of the damping mechanical resonator.

III. OPTOMECHANICAL INDUCED ANTI- \mathcal{PT} SYMMETRY BREAKING

In order to observe anti- \mathcal{PT} symmetry breaking in the single mechanical resonators, we propose to regulate the

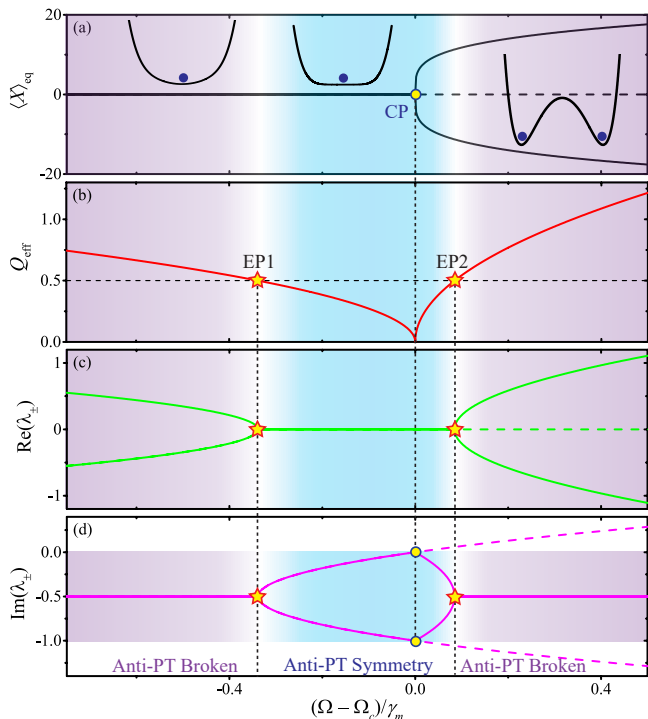


FIG. 2. (Color online) (a) Equilibrium positions of the dimensionless displacement $\langle X \rangle_{\text{eq}}$ (effective potentials U_{eff} in the insets), (b) effective quality factor Q_{eff} , (c) real parts of λ_{\pm} , and (d) imaginary parts of λ_{\pm} , versus the driving strength Ω .

effective frequency of the mechanical resonator by the optical spring effect in this section. Optomechanical systems possessing interactions between light and mechanical resonators provide an ideal platform to observe the mechanical anti- \mathcal{PT} symmetry breaking [68]. We consider a mechanical resonator coupled to an optical mode (A and A^\dagger , with frequency ω_c) through quadratic optomechanical interaction, and the optical mode is driven resonantly by an external field with strength Ω and frequency $\omega_L = \omega_c$. In a rotating frame with respect to $\hbar\omega_L A^\dagger A$, the Hamiltonian of the system reads

$$H_{\text{OM}} = \frac{p^2}{2M} + \frac{1}{2}(k + 2g_0 A^\dagger A)x^2 + \hbar\Omega (A^\dagger + A), \quad (5)$$

where $2g_0 A^\dagger A$ is the spring constant induced by the optical mode with the single-photon quadratic optomechanical coupling strength g_0 .

The quadratic optomechanical interaction has been demonstrated in various cavity-optomechanical systems, including mechanical resonator (membrane [69–72], nanosphere [73–75], cold atoms [76]) trapped in Fabry-Perot cavities, or coupled to whispering-gallery-mode [77–79] or photonic crystal cavities [80, 81]. For reality, we take the experimental parameters in our simulations for a planar silicon photonic crystal optomechanical cavity [81] with $g_0 = -6.06 \times 10^{-4}$ N/m, $M = 3.6$ pg, $\omega_m/2\pi = 8.7$ MHz, $Q_m = 10^4$, and optical damping

rate $\gamma_c/2\pi = 5$ GHz, i.e., corresponding to the sideband-unresolved regime $\gamma_c \gg \omega_m$. The motions of the mechanical resonator can be measured by a weak probe beam bypass the cavity, and the power spectra of the weak probe beam exhibits the eigenfrequency of the mechanical resonator [72]. But it should be pointed out that the negative frequency can not measured directly.

The dynamic behaviors of the mechanical resonator with quadratic optomechanical coupling can be analyzed based on the equilibrium positions obtained from the equations of motion: $d\langle x \rangle/dt = \langle p \rangle/M$ and $d\langle p \rangle/dt = -k'\langle x \rangle - \gamma_m\langle p \rangle$. Here, $k' = k + 2g_0\Omega^2/[(\gamma_c/2)^2 + (\langle x \rangle^2 g_0/\hbar)^2]$ is a position-dependent spring constant obtained by adiabatically eliminating the optical mode in the sideband-unresolved regime (see A for details). By introducing an effective potential $U_{\text{eff}} \equiv \int_0^{\langle x \rangle} k' \langle x' \rangle d\langle x' \rangle$, the equilibrium positions of the mechanical resonator are obtained under the conditions $dU_{\text{eff}}/d\langle x \rangle = 0$ and $d^2U_{\text{eff}}/d\langle x \rangle^2 \geq 0$. The equilibrium positions are shown in Figure 2(a) with the effective potentials U_{eff} in the insets. There is one equilibrium position at $\langle x \rangle_{\text{eq}} = 0$ under the critical driving $\Omega \leq \Omega_c = \sqrt{-k\gamma_c^2/(8g_0)}$, and the bottom of potential becomes more and more flat (i.e., the spring softens) with the increasing driving strength Ω . When $\Omega > \Omega_c$, the position $\langle x \rangle = 0$ becomes unstable, and the effective potential is transformed into a double well with two new equilibrium positions at $\langle x \rangle_{\text{eq}} = \pm(-\hbar/g_0)^{1/2}[-(2g_0\Omega^2/k) - (\gamma_c^2/4)]^{1/4}$.

To further analyze the motional feature of the mechanical resonator, we consider the small oscillation near its equilibrium positions $\langle x \rangle_{\text{eq}}$. Thus, we have the effective spring constants $k_{\text{eff}} = k(1 - \Omega^2/\Omega_c^2)$ for $\Omega \leq \Omega_c$ and $k_{\text{eff}} = 4k(1 - \Omega_c^2/\Omega^2)$ for $\Omega > \Omega_c$. With the increase of the driving strength Ω , the effective quality factor $Q_{\text{eff}} \equiv \omega_{\text{eff}}/\gamma_m$ with $\omega_{\text{eff}} \equiv \sqrt{k_{\text{eff}}/M}$ monotonously decreases for $\Omega \leq \Omega_c$, and then monotonically increases when $\Omega > \Omega_c$ [Figure 2(b)]. The EPs can be demonstrated from the eigenvalues in Eq. (3) with Q_m replaced by Q_{eff} [Figures 2(c) and 2(d)]. There is one EP (EP1) under the critical driving $\Omega \leq \Omega_c$. With the increase of Ω , the EP1, corresponding to the transition from the anti- \mathcal{PT} -broken to anti- \mathcal{PT} -symmetry phases appears for $Q_{\text{eff}} = 0.5$ at the optical driving strength

$$\Omega_{\text{EP1}} = \Omega_c (1 - Q_m^{-2}/4)^{1/2}. \quad (6)$$

When the driving strength continues to increase ($\Omega > \Omega_c$), another EP (EP2), corresponding to the transition from the anti- \mathcal{PT} -symmetry to anti- \mathcal{PT} -broken phases, appears at

$$\Omega_{\text{EP2}} = \Omega_c (1 - Q_m^{-2}/16)^{-1/2} \quad (7)$$

for $Q_{\text{eff}} = 0.5$. It is worth noting that the conditions for the mechanical EPs are derived analytically by adiabatically eliminating the optical mode. In order to justify the validity of the method, we show that these results are in very good agreement with the prediction without making the adiabatical approximation (see B for more details).

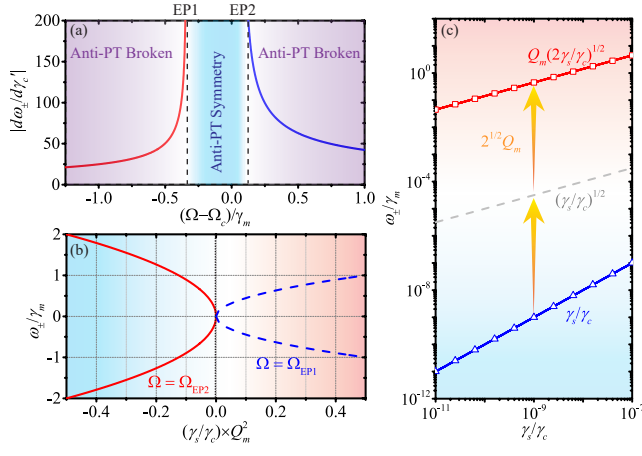


FIG. 3. (Color online) (a) The sensitivity $|d\omega_{\pm}/d\gamma'_c|$ versus the driving strength Ω . (b) Dependence of the frequency splittings ω_{\pm} on the scattering loss γ_s at EP1 (blue dashed curve for $\Omega = \Omega_{EP1}$) and EP2 (red solid curve for $\Omega = \Omega_{EP2}$). (c) The comparison among $\omega_{\pm} = \sqrt{2}Q_m\sqrt{\gamma_s/\gamma_c}$, $\sqrt{\gamma_s/\gamma_c}$, and γ_s/γ_c .

The quadratic optomechanical system can not only be used to exhibit the anti- \mathcal{PT} symmetry breaking, but also inspire a research for highly sensitive sensing based on the EPs. The frequency bifurcating around the EP in the anti- \mathcal{PT} broken phase provides a sensitive way to detect the small variations of the parameters caused by an external perturbation.

IV. OPTOMECHANICAL ANTI- \mathcal{PT} SENSOR

High sensitivity is a long-term pursue goal due to the vital importance in both fundamental and applied physics. As one of the most attractive points, the anti- \mathcal{PT} symmetry breaking provides a method to enhance the sensitivity for sensing based on the frequency bifurcating around the EPs [21, 49, 58, 86–88]. In the presence of a nanoparticle (scatterer) located around the optical cavity, one part of the optical mode field scatters into the environment, creating an addition damping, i.e., particle-induced scattering loss γ_s , which provides a physical mechanism for single nanoparticle detection [89]. Here, we consider a quadratic optomechanical system for sensing the particle-induced scattering loss γ_s based on the frequency bifurcating around the EPs. We will show that the sensitivity can be enhanced sharply around the EPs.

By considering the scattering loss γ_s induced by a single nanoparticle, the total loss of the optical mode is given by $\gamma'_c = \gamma_c + \gamma_s$. The sensitivity of the frequency splitting $\omega_{\pm} \equiv \text{Re}(\lambda_{\pm}\gamma_m)$ on the particle-induced optical scattering loss γ_s can be described by the derivative of

ω_{\pm} with respect to γ'_c as (see C for details)

$$\frac{d\omega_{\pm}}{d\gamma'_c} = \begin{cases} \pm \frac{\omega_{\pm}^2}{\Omega_c^2} \frac{1}{\gamma'_c}, & \Omega < \Omega_{EP1}, \\ 0, & \Omega_{EP1} < \Omega < \Omega_{EP2}, \\ \mp \frac{4\omega_{\pm}^2}{\Omega_c^2} \frac{1}{\gamma'_c}, & \Omega > \Omega_{EP2}, \end{cases} \quad (8)$$

where ω_{\pm} are shown in Eq. (C1) and $\Omega'_c = \sqrt{-k\gamma_c^2/(8g_0)}$. The sensitivity is enhanced sharply as the driving strength going close to the EPs, and it becomes divergent as $|\omega_{\pm}| \rightarrow 0$ at the two EPs [Figure 2(c)]. The sensitivities $|d\omega_{\pm}/d\gamma'_c|$ around the EPs are shown in Figure 3(a).

The dependence of the frequency splittings ω_{\pm} on the scattering loss γ_s ($|\gamma_s| \ll \gamma_c$) is determined by the driving strength Ω . When Ω reaches the two EPs, the frequency splittings ω_{\pm} are approximately given by

$$\frac{\omega_{\pm}}{\gamma_m} \approx \begin{cases} \pm\sqrt{2}Q_m\sqrt{\frac{\gamma_s}{\gamma_c}}, & \Omega = \Omega_{EP1}, \gamma_s > 0, \\ \pm 2\sqrt{2}Q_m\sqrt{\frac{-\gamma_s}{\gamma_c}}, & \Omega = \Omega_{EP2}, \gamma_s < 0. \end{cases} \quad (9)$$

We show the dependence of the frequency splittings ω_{\pm} on the scattering loss γ_s in Figure 3(b), corresponding to $\Omega = \Omega_{EP1}$ (blue dashed curves) and $\Omega = \Omega_{EP2}$ (red solid curves). As ω_{\pm}/γ_m depend on the square root of $|\gamma_s|/\gamma_c$, the sensitivity can be enhanced sharply when $|\gamma_s|/\gamma_c \ll 1$. Moreover, the factor Q_m in Eq. (9) can further enhance the sensitivity significantly for the mechanical resonator in the cryogenic vacuum conditions with a high quality factor Q_m ranging from 10^4 to 10^7 [69–81].

To highlight the sensing enhancement based on EPs, we compare the frequency splittings ω_{\pm} corresponding to the driving strength around or far away from the EPs. The frequency splittings ω_{\pm} for the driving strength far away from the EPs become

$$\frac{\omega_{\pm}}{\gamma_m} \approx \begin{cases} \pm Q_{\text{eff}} \left(1 + \zeta \frac{\gamma_s}{\gamma_c}\right), & \Omega_{EP1} - \Omega \gg \gamma_m, \\ \pm Q_{\text{eff}} \left(1 - \zeta' \frac{\gamma_s}{\gamma_c}\right), & \Omega - \Omega_{EP2} \gg \gamma_m, \end{cases} \quad (10)$$

where $\zeta \equiv (\Omega^2/\Omega_c)^2/[1 - (\Omega/\Omega_c)^2]$, $\zeta' \equiv (\Omega_c^2/\Omega)^2/[1 - (\Omega_c/\Omega)^2]$, and Q_{eff} depends on the driving strength Ω . There are two main differences in the expressions of the frequency splittings ω_{\pm} for the driving strength close to and far away from the EPs. Firstly, ω_{\pm} depend on the square root of the scattering loss γ_s for the driving strength close to the EPs, while ω_{\pm} depend linearly on the scattering loss γ_s for the driving strength far away from the EPs. Secondly, there is an enhancement factor Q_m in the expressions of ω_{\pm} for the driving strength close to the EPs, and Q_m is replaced by Q_{eff} for the driving strength far away from the EPs.

To show the sensing enhancement more clearly, the comparison among $\omega_{\pm} = \sqrt{2}Q_m\sqrt{\gamma_s/\gamma_c}$, $\sqrt{\gamma_s/\gamma_c}$, and γ_s/γ_c are shown in Figure 3(c). For $\gamma_s/\gamma_c = 10^{-8}$, $\sqrt{\gamma_s/\gamma_c}$ are four orders of magnitude greater than γ_s/γ_c . For $Q_m = 10^4$, ω_{\pm} are enhanced by four orders of magnitude for $Q_m\sqrt{\gamma_s/\gamma_c}$ in comparing with $\sqrt{\gamma_s/\gamma_c}$. Based

on these two physical mechanisms, the ultra-sensitive sensing can be realized based on the frequency splittings around the EPs for the driving strength close to the EPs. Similar mechanisms can be used to enhance the sensitivity for other optomechanical sensors [90–96].

V. CONCLUSION

In conclusion, we have revealed the hidden anti- \mathcal{PT} symmetry breaking, which determines the phase transition from the over-damping to under-damping states in a damping linear resonator. We have also found that the critical-damping state corresponds to the EP. In addition, we have proposed an optomechanical platform to exhibit this phase transition and exploited its application in ultra-sensitive sensing based on the frequency splittings around the EPs. The physical principle between the anti- \mathcal{PT} symmetry breaking and the damping-state phase transition is universal, and it governs the behaviors of all the damping linear resonant systems in physics, mechanics, chemistry, and biology. This work will open the door for exploring the wide applications [42–67] of anti- \mathcal{PT} symmetry in single damping linear resonators, and motivate the related studies on high-order EPs [97–101] and non-Hermitian topological physics [102–105].

Note added. After finishing this work, we note a related paper by Liang, Tang, Xu, and Liu [106], which has been published in Physical Review Letters recently. Liang *et al.* [106] proposed a scheme to realize a \mathcal{PT} -symmetry in a general dissipative resonance system by constructing a quadrature measurement-feedback loop, and demonstrated the proposal experimentally in a thermal atomic ensemble. Nevertheless, here we find that the dynamical Hamiltonian matrix of a damping linear resonator is anti- \mathcal{PT} symmetric, without resort to a feedback loop, and show that the anti- \mathcal{PT} symmetry breaking determines the phase transition from the over-damping to under-damping states.

ACKNOWLEDGMENTS

This work was supported by the National Natural Science Foundation of China (Grant Nos. 12064010, 12247105, 12175061, 11935006, 11774086, 1217050862, and 11775075), the Natural Science Foundation of Hunan Province (Grant No. 2021JJ20036), and the science and technology innovation Program of Hunan Province (Grant Nos. 2022RC1203, 2020RC4047, 2021RC4029).

Appendix A: Optomechanical induced mechanical anti- \mathcal{PT} symmetry breaking

In this section, we demonstrate the mechanical anti- \mathcal{PT} symmetry breaking in a quadratic optomechanical system. We introduce the quadratic optomechanical

model and the quantum Langevin equations in Appendix A 1, derive the equilibrium positions of the mechanical resonator in Appendix A 2, and show the anti- \mathcal{PT} symmetry breaking and the associated EPs in Appendix A 3.

1. The quadratic optomechanical model and the quantum Langevin equations

We consider a mechanical resonator (with displacement x , momentum p , mass M , spring constant k , and resonant frequency $\omega_m = \sqrt{k/M}$) coupled to an optical mode (with annihilation operator A , creation operator A^\dagger , and resonant frequency ω_c) through a quadratical optomechanical interaction. The optical mode is driven by an external field with strength Ω and frequency ω_L . The Hamiltonian of the system reads

$$H_{\text{sys}} = \hbar\omega_c A^\dagger A + \frac{p^2}{2M} + \frac{1}{2}kx^2 + g_0 A^\dagger A x^2 + \hbar\Omega (e^{-i\omega_L t} A^\dagger + e^{i\omega_L t} A), \quad (\text{A1})$$

where g_0 is the single-photon quadratic optomechanical coupling strength. Below we consider the case where the optical mode is driven resonantly, i.e., $\omega_L = \omega_c$. Then in a rotating frame with respect to $\hbar\omega_L A^\dagger A$, the Hamiltonian (A1) becomes

$$H_{\text{OM}} = \frac{p^2}{2M} + \frac{1}{2}(k + 2g_0 A^\dagger A)x^2 + \hbar\Omega (A^\dagger + A). \quad (\text{A2})$$

In this work, we assume that the optical driving field is strong (i.e., $\Omega \gg \gamma_c$, γ_c is the damping rate of the optical mode), and that the system works in the sideband-unresolved regime $\gamma_c \gg \omega_m$, which are consistent with the experimental parameters reported in the quadratic optomechanical systems [69–71, 73–81].

By adding both the dissipation terms and the corresponding noise operators with zero expectation value into the Heisenberg equations of motion, we obtain the quantum Langevin equations for the system operators as

$$\frac{dA}{dt} = -\frac{\gamma_c}{2}A - i\frac{g_0}{\hbar}Ax^2 - i\Omega + \sqrt{\gamma_c}A_{\text{in}}, \quad (\text{A3a})$$

$$\frac{dx}{dt} = \frac{p}{M}, \quad (\text{A3b})$$

$$\frac{dp}{dt} = -(k + 2g_0 A^\dagger A)x - \gamma_m p + F, \quad (\text{A3c})$$

where A_{in} is the optical input noise operator, F is the stochastic force, and γ_m is the mechanical damping rate. For the mechanical resonator, its quality factor is defined by $Q_m \equiv \omega_m/\gamma_m$.

2. Equilibrium positions of the mechanical resonator

Before investigating the dynamic behaviors of the mechanical resonator, let us derive the equilibrium posi-

tions of the mechanical resonator, which can be obtained by analyzing the expectation values of the operators in the dynamical equations (A3). Based on the factorization assumptions $\langle Ax^2 \rangle = \langle A \rangle \langle x \rangle^2$ and $\langle A^\dagger Ax \rangle = |\langle A \rangle|^2 \langle x \rangle$ [68, 85], the expectation values of these operators satisfy the following classical equations of motion

$$\frac{d\langle A \rangle}{dt} = -\frac{\gamma_c}{2} \langle A \rangle - i\frac{g_0}{\hbar} \langle A \rangle \langle x \rangle^2 - i\Omega, \quad (\text{A4a})$$

$$\frac{d\langle x \rangle}{dt} = \frac{\langle p \rangle}{M}, \quad (\text{A4b})$$

$$\frac{d\langle p \rangle}{dt} = -\left(k + 2g_0 |\langle A \rangle|^2\right) \langle x \rangle - \gamma_m \langle p \rangle. \quad (\text{A4c})$$

Below, we focus on the behaviors of the mechanical resonator by appropriately eliminating the optical mode. In the sideband-unresolved regime in which the relaxation time of the optical mode is much shorter than the oscillating period of the mechanical resonator, the optical mode can be eliminated adiabatically by setting $d\langle A \rangle/dt = 0$ in Eq. (A4a), then we obtain

$$\langle A \rangle = \frac{-i\Omega}{\frac{\gamma_c}{2} + i\frac{g_0}{\hbar} \langle x \rangle^2}. \quad (\text{A5})$$

By substituting Eq. (A5) into Eq. (A4c), the dynamic equation for the expectation value of the momentum can be obtained as

$$\frac{d\langle p \rangle}{dt} = -k' \langle x \rangle - \gamma_m \langle p \rangle, \quad (\text{A6})$$

where we introduce a position-dependent string constant

$$k' \equiv k + \frac{2g_0\Omega^2}{\left(\frac{\gamma_c}{2}\right)^2 + \left(\frac{g_0}{\hbar} \langle x \rangle^2\right)^2}. \quad (\text{A7})$$

It is worth mentioning that the string constant k' depends also on the external optical driving strength Ω , which provides an approach to regulate the behaviors of the mechanical resonator on demand.

To further analyze the motional feature of the effective mechanical resonator, we seek for the effective potential to understand both the equilibrium position of the mechanical resonator and the action of the quadratic optomechanical interaction on the mechanical motion. The effective potential is defined by $dU_{\text{eff}}/d\langle x \rangle \equiv k' \langle x \rangle$, which is obtained analytically as

$$U_{\text{eff}} = \frac{1}{2}k \langle x \rangle^2 + \frac{2\hbar\Omega^2}{\gamma_c} \arctan\left(\frac{2g_0 \langle x \rangle^2}{\hbar\gamma_c}\right) \quad (\text{A8})$$

with the zero-potential energy position at $\langle x \rangle = 0$. To present an intuitive understanding, we show the effective potential U_{eff} of the mechanical resonator versus both the driving strength Ω and dimensionless position $\langle X \rangle \equiv \langle x \rangle/(\sqrt{2}x_{\text{zp}})$ in Figure 4, where $x_{\text{zp}} = \sqrt{\hbar/(2M\omega_m)}$ and the positions for the minimums of the potential energy

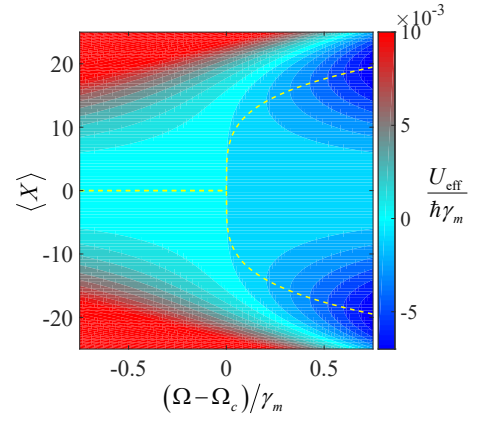


FIG. 4. (Color online) The effective potential $U_{\text{eff}}/(\hbar\gamma_m)$ of the mechanical resonator versus both the driving strength Ω and the position $\langle X \rangle$. The equilibrium position $\langle X \rangle_{\text{eq}}$ of the mechanical resonator is shown for reference (yellow dashed curves). Other parameters are: $g_0 = -6.06 \times 10^{-4}$ N/m, $M = 3.6$ pg, $\omega_m/2\pi = 8.7$ MHz, $Q_m = 10^4$, and $\gamma_c/2\pi = 5$ GHz.

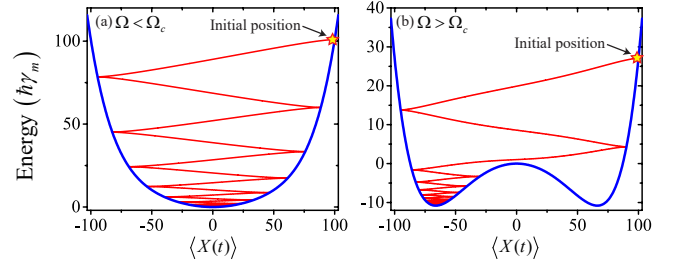


FIG. 5. (Color online) Relaxation of a mechanical resonator in (a) a single-well potential for $\Omega = \Omega_c - 100\gamma_m$ and (b) a double-well potential for $\Omega = \Omega_c + 100\gamma_m$. The initial conditions are $\langle X(0) \rangle = 100$, $\langle p(0) \rangle = 0$, and $\langle A(0) \rangle = -i\Omega/[(\gamma_c/2) + i(g_0/\hbar)\langle x(0) \rangle^2]$. The blue curves are the effective potential $U_{\text{eff}}/(\hbar\gamma_m)$ of the mechanical resonator given by Eq. (A8), and the red curves are the total energy of the mechanical resonator decaying with time. Other parameters are the same as those used in Figure 4.

(i.e., the equilibrium position $\langle X \rangle_{\text{eq}}$ discussed in the following) are shown by yellow dashed curves. In Figure 5, we show the dynamics of the mechanical resonator based on the nonlinear equations of motion for the expectation values, i.e., Eq. (A4). It is clear that the mechanical resonator oscillates with damping amplitude in a single-well potential for $\Omega < \Omega_c$ or in a double-well potential for $\Omega > \Omega_c$, which agree well with the effective potential given by Eq. (A8).

The equilibrium position $\langle x \rangle_{\text{eq}}$ is obtained for the potential energy satisfying the conditions $dU_{\text{eff}}/d\langle x \rangle = 0$ and $d^2U_{\text{eff}}/d\langle x \rangle^2 \geq 0$. From the condition $dU_{\text{eff}}/d\langle x \rangle = 0$, we have either

$$\langle x \rangle_{\text{eq}} = 0, \quad (\text{A9})$$

or

$$\langle x \rangle_{\text{eq}} = \pm \sqrt{-\frac{\hbar}{g_0} \sqrt{-\frac{2g_0\Omega^2}{k} - \left(\frac{\gamma_c}{2}\right)^2}} \quad (\text{A10})$$

for $g_0 < 0$ and $\Omega > \Omega_c$. Here, the critical driving strength is defined by

$$\Omega_c = \sqrt{\frac{k\gamma_c^2}{8g_0}}. \quad (\text{A11})$$

From the condition $d^2U_{\text{eff}}/d\langle x \rangle^2 \geq 0$, we have

$$k + \frac{2g_0\Omega^2}{\left(\frac{\gamma_c}{2}\right)^2 + \left(\frac{g_0}{\hbar}\langle x \rangle^2\right)^2} - \frac{8g_0\Omega^2 \left(\frac{g_0}{\hbar}\langle x \rangle^2\right)^2}{\left[\left(\frac{\gamma_c}{2}\right)^2 + \left(\frac{g_0}{\hbar}\langle x \rangle^2\right)^2\right]^2} \geq 0. \quad (\text{A12})$$

Thus, $\langle x \rangle_{\text{eq}} = 0$ is stable only when the driving strength $\Omega \leq \Omega_c$, namely the single-well regime. When the driving strength $\Omega > \Omega_c$, $\langle x \rangle = 0$ becomes unstable (see Figure 4), and there are two stable equilibrium positions at

$$\langle x \rangle_{\text{eq}} = \pm \sqrt{-\frac{\hbar}{g_0} \sqrt{-\frac{2g_0\Omega^2}{k} - \left(\frac{\gamma_c}{2}\right)^2}}, \text{ i.e., the double-well regime.}$$

To sum up, we have the equilibrium positions

$$\langle x \rangle_{\text{eq}} = \begin{cases} 0, & \Omega \leq \Omega_c, \\ \pm \sqrt{-\frac{\hbar}{g_0} \sqrt{-\frac{2g_0\Omega^2}{k} - \left(\frac{\gamma_c}{2}\right)^2}}, & \Omega > \Omega_c. \end{cases} \quad (\text{A13})$$

Meanwhile, the average photon number corresponding to the mechanical resonator in the equilibrium position read

$$|\langle A \rangle_{\text{eq}}|^2 = \begin{cases} \frac{4\Omega^2}{\gamma_c^2}, & \Omega \leq \Omega_c, \\ \frac{4\Omega_c^2}{\gamma_c^2}, & \Omega > \Omega_c. \end{cases} \quad (\text{A14})$$

Under the parameters in Figure 4, we have the average photon number $|\langle A \rangle_{\text{eq}}|^2 \approx 8875.6$ for $\Omega = \Omega_c$, which is not strong enough to consider the intrinsic nonlinear phenomena in the optical cavity [107]. We have checked that both the equilibrium positions $\langle x \rangle_{\text{eq}}$ and the corresponding cavity coherent amplitude $\langle A \rangle_{\text{eq}}$ are also the steady-state solutions of the equations of classical motion [Eqs. (A4)].

3. Anti- \mathcal{PT} symmetry breaking and the EPs

In this subsection, we analyze the motional feature of the mechanical resonator around the equilibrium position $\langle x \rangle_{\text{eq}}$ to show the anti- \mathcal{PT} symmetry breaking and the associated EPs. The dynamical equations for $\langle x \rangle$ and $\langle p \rangle$ around the equilibrium position $\langle x \rangle_{\text{eq}}$ can be obtained under the replacement: $\langle x \rangle \rightarrow \langle x \rangle_{\text{eq}} + \langle x \rangle$ and $\langle p \rangle \rightarrow \langle p \rangle$

(for $\langle q \rangle_{\text{eq}} = 0$), as

$$\frac{d\langle x \rangle}{dt} = \frac{\langle p \rangle}{M}, \quad (\text{A15a})$$

$$\frac{d\langle p \rangle}{dt} = -k_{\text{eff}}\langle x \rangle - \gamma_m\langle p \rangle, \quad (\text{A15b})$$

where we introduce the effective spring constant

$$k_{\text{eff}} = \begin{cases} k \left(1 - \frac{\Omega^2}{\Omega_c^2}\right), & \Omega \leq \Omega_c, \\ 4k \left(1 - \frac{\Omega_c^2}{\Omega^2}\right), & \Omega > \Omega_c \end{cases} \quad (\text{A16})$$

around the equilibrium positions. Based on the relations

$$x = x_{\text{zp}}(b^\dagger + b), \quad p = ip_{\text{zp}}(b^\dagger - b) \quad (\text{A17})$$

with $p_{\text{zp}} = \sqrt{\hbar M \omega_m / 2}$, the dynamical equations for $\langle x \rangle$ and $\langle p \rangle$ can also be rewritten as the dynamical equations for exception values of the bosonic annihilation operator b and creation operator b^\dagger in a matrix form as

$$i \frac{d}{dt} \begin{pmatrix} \langle b \rangle \\ \langle b^\dagger \rangle \end{pmatrix} = H_{\text{eff}} \begin{pmatrix} \langle b \rangle \\ \langle b^\dagger \rangle \end{pmatrix}. \quad (\text{A18})$$

Here, the dynamical Hamiltonian matrix for the effective mechanical resonator is given by

$$\frac{H_{\text{eff}}}{\hbar\gamma_m} = \begin{pmatrix} Q_{\text{eff}} - i/2 & i/2 \\ i/2 & -Q_{\text{eff}} - i/2 \end{pmatrix}, \quad (\text{A19})$$

and the corresponding eigenvalues are given by

$$\lambda_{\pm} = -i/2 \pm \sqrt{Q_{\text{eff}}^2 - 1/4}, \quad (\text{A20})$$

where $Q_{\text{eff}} \equiv \omega_{\text{eff}}/\gamma_m$ is the quality factor of the effective mechanical resonator. The H_{eff} [Eq. (A19)] is the same as the one for a simple mechanical resonator [Eq. (1) in the main text], except that the quality factor Q_m is replaced by the effective quality factor Q_{eff} . Importantly, the value of Q_{eff} depends on the driving strength Ω , which provides an effective way to demonstrate both the mechanical anti- \mathcal{PT} symmetry breaking and the EPs.

The driving strengths for the EPs can be given analytically for the system working around the equilibrium position $\langle x \rangle_{\text{eq}}$. In the single-well regime ($\Omega \leq \Omega_c$), we have $\langle x \rangle_{\text{eq}} = 0$ and $\omega_{\text{eff}} = \sqrt{k_{\text{eff}}/M}$ with $k_{\text{eff}} = k \left(1 - \frac{\Omega^2}{\Omega_c^2}\right)$. There is one EP (EP1) at $Q_{\text{eff}} = 0.5$, and we can get the driving strength for EP1 as

$$\Omega_{\text{EP1}} = \Omega_c \left[1 - \left(\frac{1}{2Q_m}\right)^2\right]^{1/2}. \quad (\text{A21})$$

In the double-well regime ($\Omega > \Omega_c$), we have $\langle x \rangle_{\text{eq}} = \pm \sqrt{-\frac{\hbar}{g_0} \sqrt{-\frac{2g_0\Omega^2}{k} - \left(\frac{\gamma_c}{2}\right)^2}}$, then another EP (EP2) appears at the driving strength

$$\Omega_{\text{EP2}} = \Omega_c \left[1 - \left(\frac{1}{4Q_m}\right)^2\right]^{-1/2}. \quad (\text{A22})$$

Appendix B: The eigenvalues of the linearized Hamiltonian without adiabatical approximation

In Appendix A 1, the mechanical EPs are derived analytically by adiabatically eliminating the optical mode based on the fact that the system works in the sideband-unresolved regime $\gamma_c \gg \omega_m$. In order to justify the validity of the method, here we calculate the eigenvalues of the linearized Hamiltonian for the quadratic optomechanical system without making the adiabatical approximation.

We expand the operators as the sum of the expectation values in the steady state (i.e., in the equilibrium position) and the quantum fluctuations: $A \rightarrow \langle A \rangle_{\text{eq}} + a$, $x \rightarrow \langle x \rangle_{\text{eq}} + x$, and $p \rightarrow p$, where a , x , and p on the right-hand side of these relations are the quantum fluctuation operators, which satisfy the quantum Langevin equations

$$\frac{da}{dt} = \left(-\frac{\gamma_c}{2} - i\Delta_{\text{eq}}\right) a - iG_{0,\text{eq}}x + \sqrt{\gamma_c}A_{\text{in}}, \quad (\text{B1a})$$

$$\frac{da^\dagger}{dt} = \left(-\frac{\gamma_c}{2} + i\Delta_{\text{eq}}\right) a^\dagger + iG_{0,\text{eq}}^*x + \sqrt{\gamma_c}A_{\text{in}}^\dagger, \quad (\text{B1b})$$

$$\frac{dx}{dt} = \frac{p}{M}, \quad (\text{B1c})$$

$$\frac{dp}{dt} = -k_{\text{eq}}x - \hbar G_{0,\text{eq}}a^\dagger - \hbar G_{0,\text{eq}}^*a - \gamma_m p + F. \quad (\text{B1d})$$

with $\Delta_{\text{eq}} \equiv \frac{g_0}{\hbar} \langle x \rangle_{\text{eq}}^2$, $G_{0,\text{eq}} \equiv 2\frac{g_0}{\hbar} \langle A \rangle_{\text{eq}} \langle x \rangle_{\text{eq}}$, and $k_{\text{eq}} \equiv k + 2g_0 \left| \langle A \rangle_{\text{eq}} \right|^2$. The equations can be rewritten with the dimensionless position $X \equiv x/(\sqrt{2}x_{\text{zp}})$ and momentum $P \equiv p/(\sqrt{2}p_{\text{zp}})$ as

$$\frac{da}{dt} = \left(-\frac{\gamma_c}{2} - i\Delta_{\text{eq}}\right) a - iG_{\text{eq}}X + \sqrt{\gamma_c}A_{\text{in}}, \quad (\text{B2a})$$

$$\frac{da^\dagger}{dt} = \left(-\frac{\gamma_c}{2} + i\Delta_{\text{eq}}\right) a^\dagger + iG_{\text{eq}}^*X + \sqrt{\gamma_c}A_{\text{in}}^\dagger, \quad (\text{B2b})$$

$$\frac{dX}{dt} = \omega_m P, \quad (\text{B2c})$$

$$\frac{dP}{dt} = -\omega'_m X - G_{\text{eq}}^*a - G_{\text{eq}}a^\dagger - \gamma_m P + \xi, \quad (\text{B2d})$$

with $\langle X \rangle_{\text{eq}} \equiv \langle x \rangle_{\text{eq}}/(\sqrt{2}x_{\text{zp}})$, $g \equiv g_0/(2M\omega_m)$, $\Delta_{\text{eq}} \equiv 2g \langle X \rangle_{\text{eq}}^2$, $G_{\text{eq}} \equiv 4g \langle A \rangle_{\text{eq}} \langle X \rangle_{\text{eq}}$, $\omega'_m \equiv \omega_m + 4g \left| \langle A \rangle_{\text{eq}} \right|^2$, and $\xi \equiv \sqrt{2}x_{\text{zp}}F/\hbar$. By defining the vectors $V \equiv (a, a^\dagger, X, P)^T$ and $V_{\text{in}} \equiv (\sqrt{\gamma_c}A_{\text{in}}, \sqrt{\gamma_c}A_{\text{in}}^\dagger, 0, \xi)^T$, the dynamical equations (B2) can be written in a matrix form as

$$\frac{d}{dt}V = -iH_{\text{OM,eff}}V + V_{\text{in}}, \quad (\text{B3})$$

where we introduce the effective optomechanical Hamil-

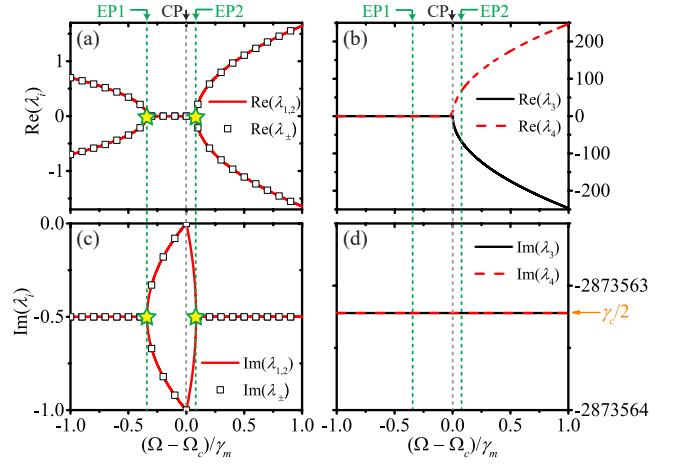


FIG. 6. (Color online) Comparison of these eigenvalues λ_i ($i = 1, 2, 3, 4$) of $H_{\text{OM,eff}}$ [Eq. (B4)] with the eigenvalues λ_{\pm} of H_{eff} [Eq. (A19)] versus the driving strength Ω : (a) and (b) real parts; (c) and (d) imaginary parts. EP1 and EP2 are given by Eqs. (A21) and (A22) and CP is given by Eq. (A11). Other parameters are: $g_0 = -6.06 \times 10^{-4}$ N/m, $M = 3.6$ pg, $\omega_m/2\pi = 8.7$ MHz, $Q_m = 10^4$, and $\gamma_c/2\pi = 5$ GHz.

tonian as

$$H_{\text{OM,eff}} = \begin{pmatrix} -i\frac{\gamma_c}{2} + \Delta_{\text{eq}} & 0 & G_{\text{eq}} & 0 \\ 0 & -i\frac{\gamma_c}{2} - \Delta_{\text{eq}} & -G_{\text{eq}}^* & 0 \\ 0 & 0 & 0 & i\omega_m \\ -iG_{\text{eq}}^* & -iG_{\text{eq}} & -i\omega'_m & -i\gamma_m \end{pmatrix}. \quad (\text{B4})$$

The eigenvalues λ_i ($i = 1, 2, 3, 4$) of $H_{\text{OM,eff}}/\gamma_m$ are the roots of the characteristic polynomial $|H_{\text{OM,eff}}/\gamma_m - \lambda I| = 0$, where I is the identity matrix.

In Figure 6, we show λ_i ($i = 1, 2, 3, 4$) and λ_{\pm} [Eq. (A20)] versus the driving strength Ω for comparison. Two of λ_i for $i = 1, 2$ are eigenvalues for the mechanical-like modes, and they are almost the same as λ_{\pm} for both real and imaginary parts, as shown in Figures 6(a) and 6(c). Here, the EPs can be confirmed with the prediction values given by Eqs. (A21) and (A22). Thus, the results in Eq. (A20), which are obtained by eliminating the optical mode adiabatically, are justified. Moreover, λ_i ($i = 3, 4$) are the eigenvalues for the optical-like modes, with the frequency bifurcation around the critical driving strength Ω_c , as denoted by CP (the abbreviation of “critical point”) in Figures 6(b) and 6(d).

Appendix C: The sensitivity for optomechanical sensing based on EPs

The EPs associated with the anti- \mathcal{PT} symmetry breaking provide a physical mechanism to enhance the sensing sensitivity in quantum sensing. Here, based on the optomechanical induced mechanical anti- \mathcal{PT} symmetry breaking, we consider ultrasensitive sensing on the scattering loss γ_s induced by a single nanoparticle with the

total loss of the optical mode given by $\gamma'_c = \gamma_c + \gamma_s$. In terms of the quadratically optomechanical interaction and under the strong optical-driving condition, the frequency splittings ω_{\pm} , i.e., the real part of the eigenvalues $\lambda_{\pm}\gamma_m$, are given by

$$\omega_{\pm} = \begin{cases} \pm\sqrt{\omega_m^2\left(1 - \frac{\Omega^2}{\Omega_c^2}\right) - \left(\frac{\gamma_m}{2}\right)^2}, & \Omega < \Omega_{\text{EP1}}, \\ 0, & \Omega_{\text{EP1}} < \Omega < \Omega_{\text{EP2}}, \\ \pm\sqrt{4\omega_m^2\left(1 - \frac{\Omega'^2}{\Omega^2}\right) - \left(\frac{\gamma_m}{2}\right)^2}, & \Omega > \Omega_{\text{EP2}}. \end{cases} \quad (\text{C1})$$

where $\Omega'_c = \sqrt{-k\gamma_c'^2/(8g_0)}$. The sensitivity of the frequency splittings ω_{\pm} on the change of the optical damping rate γ'_c can be described by the derivative of ω_{\pm} with respect to γ'_c as

$$\frac{d\omega_{\pm}}{d\gamma'_c} = \begin{cases} \pm\frac{\omega_m^2}{\omega_{\pm}}\frac{\Omega^2}{\Omega_c^2}\frac{1}{\gamma'_c}, & \Omega < \Omega_{\text{EP1}}, \\ 0, & \Omega_{\text{EP1}} < \Omega < \Omega_{\text{EP2}}, \\ \mp\frac{4\omega_m^2}{\omega_{\pm}}\frac{\Omega_c'^2}{\Omega^2}\frac{1}{\gamma'_c}, & \Omega > \Omega_{\text{EP2}}, \end{cases} \quad (\text{C2})$$

where ω_{\pm} are shown in Eq. (C1).

The dependence of the frequency splittings ω_{\pm} on the scattering loss γ_s is determined by the driving strength

Ω . Under the assumption that $\gamma_s \ll \gamma_c$, we have

$$\frac{\omega_{\pm}}{\gamma_m} \approx \begin{cases} \pm\sqrt{Q_{\text{eff}}^2 - \frac{1}{4} + 2Q_m^2\frac{\Omega^2}{\Omega_c^2}\frac{\gamma_s}{\gamma_c}}, & \Omega < \Omega_{\text{EP1}}, \\ 0, & \Omega_{\text{EP1}} < \Omega < \Omega_{\text{EP2}}, \\ \pm\sqrt{Q_{\text{eff}}^2 - \frac{1}{4} - 8Q_m^2\frac{\Omega_c'^2}{\Omega^2}\frac{\gamma_s}{\gamma_c}}, & \Omega > \Omega_{\text{EP2}}, \end{cases} \quad (\text{C3})$$

where $Q_{\text{eff}} = Q_m\sqrt{1 - (\Omega/\Omega_c)^2}$ for $\Omega < \Omega_{\text{EP1}}$ and $Q_{\text{eff}} = 2Q_m\sqrt{1 - (\Omega_c/\Omega)^2}$ for $\Omega > \Omega_{\text{EP2}}$. To show the sensing enhancement by the EPs, we compare the frequency splittings ω_{\pm} for the driving strength around the EPs with the results for the driving strength far away from the EPs. We have $Q_{\text{eff}} = 0.5$ for both $\Omega = \Omega_{\text{EP1}}$ and $\Omega = \Omega_{\text{EP2}}$, so the frequency splittings ω_{\pm} around the two EPs are approximately given by

$$\frac{\omega_{\pm}}{\gamma_m} \approx \begin{cases} \pm\sqrt{2}Q_m\sqrt{\frac{\gamma_s}{\gamma_c}}, & \Omega = \Omega_{\text{EP1}}, \gamma_s > 0, \\ \pm 2\sqrt{2}Q_m\sqrt{\frac{-\gamma_s}{\gamma_c}}, & \Omega = \Omega_{\text{EP2}}, \gamma_s < 0, \end{cases} \quad (\text{C4})$$

for $\Omega_{\text{EP1}}/\Omega_c \approx \Omega_c/\Omega_{\text{EP2}} \approx 1$. Instead, we have $Q_{\text{eff}} \gg 0.5$ for $(\Omega_{\text{EP1}} - \Omega) \gg \gamma_m$ or $(\Omega - \Omega_{\text{EP2}}) \gg \gamma_m$, then the frequency splittings ω_{\pm} corresponding to the driving strength Ω far away from the two EPs are shown as

$$\frac{\omega_{\pm}}{\gamma_m} \approx \begin{cases} \pm Q_{\text{eff}}\left(1 + \zeta\frac{\gamma_s}{\gamma_c}\right), & \Omega_{\text{EP1}} - \Omega \gg \gamma_m, \\ \pm Q_{\text{eff}}\left(1 - \zeta'\frac{\gamma_s}{\gamma_c}\right), & \Omega - \Omega_{\text{EP2}} \gg \gamma_m, \end{cases} \quad (\text{C5})$$

where $\zeta \equiv (\Omega^2/\Omega_c^2)/[1 - (\Omega/\Omega_c)^2]$ and $\zeta' \equiv (\Omega_c'^2/\Omega^2)/[1 - (\Omega_c/\Omega)^2]$.

-
- [1] F. S. Crawford Jr., “Waves (In SI Units), Berkeley Physics Course-Volume 3” (McGraw-Hill Asia Holdings (Singapore) PTE. LTD and China Machine, 2014).
- [2] H.-P. Breuer and F. Petruccione, “The Theory of Open Quantum Systems” (Oxford University Press, Oxford, 1993).
- [3] C. M. Bender and S. Boettcher, “Real spectra in non-hermitian hamiltonians having \mathcal{PT} symmetry”, *Phys. Rev. Lett.* **80**, 5243 (1998).
- [4] C. M. Bender, “Making sense of non-Hermitian Hamiltonians”, *Rep. Prog. Phys.* **70**, 947 (2007).
- [5] V. V. Konotop, J. Yang, and D. A. Zezyulin, “Nonlinear waves in \mathcal{PT} -symmetric systems”, *Rev. Mod. Phys.* **88**, 035002 (2016).
- [6] R. El-Ganainy, K. G. Makris, M. Khajavikhan, Z. H. Musslimani, S. Rotter, and D. N. Christodoulides, “Non-Hermitian physics and \mathcal{PT} symmetry”, *Nat. Phys.* **14**, 11 (2018).
- [7] H. Wang, X. Zhang, J. Hua, D. Lei, M. Lu, and Y. Chen, “Topological physics of non-Hermitian optics and photonics: a review”, *J. Opt.* **23**, 123001 (2021).
- [8] A. Guo, G. J. Salamo, D. Duchesne, R. Morandotti, M. Volatier-Ravat, V. Aimez, G. A. Siviloglou, and D. N. Christodoulides, “Observation of \mathcal{PT} -symmetry breaking in complex optical potentials”, *Phys. Rev. Lett.* **103**, 093902 (2009).
- [9] C. E. Rüter, K. G. Makris, R. El-Ganainy, D. N. Christodoulides, M. Segev, and D. Kip, “Observation of parity-time symmetry in optics”, *Nat. Phys.* **6**, 192 (2010).
- [10] Z. Lin, H. Ramezani, T. Eichelkraut, T. Kottos, H. Cao, and D. N. Christodoulides, “Unidirectional invisibility induced by \mathcal{PT} -symmetric periodic structures”, *Phys. Rev. Lett.* **106**, 213901 (2011).
- [11] H. Jing, S. K. Özdemir, X.-Y. Lü, J. Zhang, L. Yang, and F. Nori, “ \mathcal{PT} -symmetric phonon laser”, *Phys. Rev. Lett.* **113**, 053604 (2014).
- [12] X.-Y. Lü, H. Jing, J.-Y. Ma, and Y. Wu, “ \mathcal{PT} -symmetry-breaking chaos in optomechanics”, *Phys. Rev. Lett.* **114**, 253601 (2015).
- [13] B. Peng, S. K. Özdemir, F. Lei, F. Monifi, M. Gianfreda, G. L. Long, S. Fan, F. Nori, C. M. Bender, and L. Yang, “Parity-time-symmetric whispering-gallery microcavities”, *Nat. Phys.* **10**, 394 (2014).
- [14] L. Chang, X. Jiang, S. Hua, C. Yang, J. Wen, L. Jiang, G. Li, G. Wang, and M. Xiao, “Parity-time symmetry and variable optical isolation in active-passive-coupled microresonators”, *Nat. Photonics* **8**, 524 (2014).
- [15] S. K. Özdemir, S. Rotter, F. Nori, and L. Yang, “Parity-time symmetry and exceptional points in photonics”,

- Nat. Mater.* **18**, 783 (2019).
- [16] M.-A. Miri and A. Alù, “Exceptional points in optics and photonics”, *Science* **363**, eaar7709 (2019).
- [17] F. Klauck, L. Teuber, M. Ornigotti, M. Heinrich, S. Scheel, and A. Szameit, “Observation of \mathcal{PT} -symmetric quantum interference”, *Nat. Photonics* **13**, 883 (2019).
- [18] B. Peng, S. K. Özdemir, S. Rotter, H. Yilmaz, M. Liertzer, F. Monifi, C. M. Bender, F. Nori, and L. Yang, “Loss-induced suppression and revival of lasing”, *Science* **346**, 328 (2014).
- [19] L. Feng, Z. J. Wong, R.-M. Ma, Y. Wang, and X. Zhang, “Single-mode laser by parity-time symmetry breaking”, *Science* **346**, 972 (2014).
- [20] Z.-P. Liu, J. Zhang, S. K. Özdemir, B. Peng, H. Jing, X.-Y. Lü, C.-W. Li, L. Yang, F. Nori, and Y.-x. Liu, “Metrology with \mathcal{PT} -symmetric cavities: Enhanced sensitivity near the \mathcal{PT} -phase transition”, *Phys. Rev. Lett.* **117**, 110802 (2016).
- [21] W. Chen, S. K. Özdemir, G. Zhao, J. Wiersig, and L. Yang, “Exceptional points enhance sensing in an optical microcavity”, *Nature (London)* **548**, 192 (2017).
- [22] H. Hodaie, A. U. Hassan, S. Wittek, H. Garcia-Gracia, R. El-Ganainy, D. N. Christodoulides, and M. Khajavikhan, “Enhanced sensitivity at higher-order exceptional points”, *Nature (London)* **548**, 187 (2017).
- [23] Q.-C. Wu, J.-L. Zhao, Y.-L. Fang, Y. Zhang, D.-X. Chen, C.-P. Yang, F. Nori, “Extension of Noether’s theorem in \mathcal{PT} -symmetry systems and its experimental demonstration in an optical setup”, *Sci. China Phys. Mech. Astron.* **66**, 240312 (2023).
- [24] C. M. Bender, B. K. Berntson, D. Parker, and E. Samuel, “Observation of \mathcal{PT} phase transition in a simple mechanical system”, *Am. J. Phys.* **81**, 173 (2013).
- [25] X. Zhu, H. Ramezani, C. Shi, J. Zhu, and X. Zhang, “ \mathcal{PT} -symmetric acoustics”, *Phys. Rev. X* **4**, 031042 (2014).
- [26] R. Fleury, D. Sounas, and A. Alù, “An invisible acoustic sensor based on parity-time symmetry”, *Nat. Commun.* **6**, 5905 (2015).
- [27] K. Ding, G. Ma, M. Xiao, Z. Q. Zhang, and C. T. Chan, “Emergence, coalescence, and topological properties of multiple exceptional points and their experimental realization”, *Phys. Rev. X* **6**, 021007 (2016).
- [28] T. Liu, X. Zhu, F. Chen, S. Liang, and J. Zhu, “Unidirectional wave vector manipulation in twodimensional space with an all passive acoustic parity-time-symmetric metamaterials crystal”, *Phys. Rev. Lett.* **120**, 124502 (2018).
- [29] J. Schindler, A. Li, M. C. Zheng, F. M. Ellis, and T. Kottos, “Experimental study of active lrc circuits with \mathcal{PT} symmetries”, *Phys. Rev. A* **84**, 040101(R) (2011).
- [30] J. Schindler, Z. Lin, J. M. Lee, H. Ramezani, F. M. Ellis, and T. Kottos, “ \mathcal{PT} -symmetric electronics”, *J. Phys. A: Math. Theor.* **45**, 444029 (2012).
- [31] X. Yang, J. Li, Y. Ding, M. Xu, X.-F. Zhu, and J. Zhu, “Observation of transient parity-time symmetry in electronic systems”, *Phys. Rev. Lett.* **128**, 065701 (2022).
- [32] Y. Sun, W. Tan, H.-q. Li, J. Li, and H. Chen, “Experimental demonstration of a coherent perfect absorber with \mathcal{PT} phase transition”, *Phys. Rev. Lett.* **112**, 143903 (2014).
- [33] S. Assaworarith, X. Yu, and S. Fan, “Robust wireless power transfer using a nonlinear parity-time-symmetric circuit”, *Nature (London)* **546**, 387 (2017).
- [34] Z. Dong, Z. Li, F. Yang, C.-W. Qiu, and J. Ho, “Sensitive readout of implantable microsensors using a wireless system locked to an exceptional point”, *Nat. Electron.* **2**, 335 (2019).
- [35] H. Liu, D. Sun, C. Zhang, M. Groesbeck, R. Mclaughlin, and Z. V. Vardeny, “Observation of exceptional points in magnonic parity-time symmetry devices”, *Sci. Adv.* **5**, eaax9144 (2019).
- [36] W.-C. Wang, Y.-L. Zhou, H.-L. Zhang, J. Zhang, M.-C. Zhang, Y. Xie, C.-W. Wu, T. Chen, B.-Q. Ou, W. Wu, H. Jing, and P.-X. Chen, “Observation of \mathcal{PT} -symmetric quantum coherence in a single-ion system”, *Phys. Rev. A* **103**, L020201 (2021).
- [37] L. Ding, K. Shi, Q. Zhang, D. Shen, X. Zhang, and W. Zhang, “Experimental determination of \mathcal{PT} -symmetric exceptional points in a single trapped ion”, *Phys. Rev. Lett.* **126**, 083604 (2021).
- [38] Y. Wu, W. Liu, J. Geng, X. Song, X. Ye, C.-K. Duan, X. Rong, and J. Du, “Observation of parity-time symmetry breaking in a single-spin system”, *Science* **364**, 878 (2019).
- [39] X. Xiao, Q.-H. Liao, N.-R. Zhou, W.-J. Nie, and Y.-C. Liu, “Tunable optical second-order sideband effects in a parity-time symmetric optomechanical system”, *Sci. China Phys. Mech. Astron.* **63**, 114211 (2020).
- [40] X. Zhang, J. Hu, and N. Zhao, “Stable atomic magnetometer in parity-time symmetry broken phase”, *Phys. Rev. Lett.* **130**, 023201 (2023).
- [41] L. Ge and H. E. Türeci, “Antisymmetric \mathcal{PT} -photonic structures with balanced positive- and negative-index materials”, *Phys. Rev. A* **88**, 053810 (2013).
- [42] J.-H. Wu, M. Artoni, and G. C. La Rocca, “Non-hermitian degeneracies and unidirectional reflectionless atomic lattices”, *Phys. Rev. Lett.* **113**, 123004 (2014).
- [43] Y. He, J. Wu, Y. Hu, J.-X. Zhang, and S.-Y. Zhu, “Unidirectional reflectionless anti-parity-timesymmetric photonic lattices of thermal atoms”, *Phys. Rev. A* **105**, 043712 (2022).
- [44] H. Xu, D. Mason, L. Jiang, and J. G. E. Harris, “Topological energy transfer in an optomechanical system with exceptional points”, *Nature (London)* **537**, 80 (2016).
- [45] J. Doppler, A. A. Mailybaev, J. Böhm, U. Kuhl, A. Girschik, F. Libisch, T. J. Milburn, P. Rabl, N. Moiseyev, and S. Rotter, “Dynamically encircling an exceptional point for asymmetric mode switching”, *Nature (London)* **537**, 76 (2016).
- [46] Y.-X. Wang and A. A. Clerk, “Non-hermitian dynamics without dissipation in quantum systems”, *Phys. Rev. A* **99**, 063834 (2019).
- [47] F. Zhang, Y. Feng, X. Chen, L. Ge, and W. Wan, “Synthetic anti- \mathcal{PT} symmetry in a single microcavity”, *Phys. Rev. Lett.* **124**, 053901 (2020).
- [48] S. Park, D. Lee, K. Park, H. Shin, Y. Choi, and J. W. Yoon, “Optical energy-difference conservation in a synthetic anti- \mathcal{PT} -symmetric system”, *Phys. Rev. Lett.* **127**, 083601 (2021).
- [49] H. Zhang, R. Huang, S.-D. Zhang, Y. Li, C.-W. Qiu, F. Nori, and H. Jing, “Breaking anti- \mathcal{PT} symmetry by spinning a resonator”, *Nano Lett.* **20**, 7594 (2020).
- [50] J.-H. Wu, M. Artoni, and G. C. La Rocca, “Parity-time-antisymmetric atomic lattices without gain”, *Phys. Rev. A* **91**, 033811 (2015).

- [51] P. Peng, W. Cao, C. Shen, W. Qu, J. Wen, L. Jiang, and Y. Xiao, “Anti-parity-time symmetry with flying atoms”, *Nat. Phys.* **12**, 1139 (2016).
- [52] Y. Jiang, Y. Mei, Y. Zuo, Y. Zhai, J. Li, J. Wen, and S. Du, “Anti-parity-time symmetric optical four-wave mixing in cold atoms”, *Phys. Rev. Lett.* **123**, 193604 (2019).
- [53] Y. Choi, C. Hahn, J. W. Yoon, and S. H. Song, “Observation of an anti- \mathcal{PT} -symmetric exceptional point and energy-difference conserving dynamics in electrical circuit resonators”, *Nat. Commun.* **9**, 2182 (2018).
- [54] Y. Li, Y.-G. Peng, L. Han, M.-A. Miri, W. Li, M. Xiao, X.-F. Zhu, J. Zhao, A. Alù, S. Fan, and C.-W. Qiu, “Anti-parity-time symmetry in diffusive systems”, *Science* **364**, 170 (2019).
- [55] F. Yang, Y.-C. Liu, and L. You, “Anti- \mathcal{PT} symmetry in dissipatively coupled optical systems”, *Phys. Rev. A* **96**, 053845 (2017).
- [56] X.-L. Zhang, T. Jiang, and C. T. Chan, “Dynamically encircling an exceptional point in anti-parity-time symmetric systems: asymmetric mode switching for symmetrybroken modes”, *Light Sci. Appl.* **8**, 88 (2019).
- [57] Q. Li, C.-J. Zhang, Z.-D. Cheng, W.-Z. Liu, J.-F. Wang, F.-F. Yan, Z.-H. Lin, Y. Xiao, K. Sun, Y.-T. Wang, J.-S. Tang, J.-S. Xu, C.-F. Li, and G.-C. Guo, “Experimental simulation of anti-parity-time symmetric Lorentz dynamics”, *Optica* **6**, 67 (2019).
- [58] Y.-H. Lai, Y.-K. Lu, M.-G. Suh, Z. Yuan, and K. Vahala, “Observation of the exceptional-point-enhanced Sagnac effect”, *Nature (London)* **576**, 65 (2019).
- [59] Z.-H. Peng, C.-X. Jia, Y.-Q. Zhang, J.-B. Yuan, and L.-M. Kuang, “Level attraction and \mathcal{PT} symmetry in indirectly coupled microresonators”, *Phys. Rev. A* **102**, 043527 (2020).
- [60] A. Bergman, R. Duggan, K. Sharma, M. Tur, A. Zadok, and A. Alù, “Observation of anti-parity-time-symmetry, phase transitions and exceptional points in an optical fibre”, *Nat. Commun.* **12**, 486 (2021).
- [61] Y. Yang, Y.-P. Wang, J. W. Rao, Y. S. Gui, B. M. Yao, W. Lu, and C.-M. Hu, “Unconventional singularity in anti-parity-time symmetric cavity magnonics”, *Phys. Rev. Lett.* **125**, 147202 (2020).
- [62] J. Zhao, Y. Liu, L. Wu, C.-K. Duan, Y.-x. Liu, and J. Du, “Observation of anti- \mathcal{PT} -symmetry phase transition in the magnon-cavity-magnon coupled system”, *Phys. Rev. Applied* **13**, 014053 (2020).
- [63] Q. Zhang, C. Yang, J. Sheng, and H. Wu, “Dissipative coupling-induced phonon lasing”, *PNAS* **119**, e2207543119 (2022).
- [64] H. Zhang, M. Peng, X.-W. Xu, and H. Jing, “Anti- \mathcal{PT} -symmetric Kerr gyroscope”, *Chin. Phys. B* **31**, 014215 (2022).
- [65] X. H. H. Zhang and H. U. Baranger, “Driven-dissipative phase transition in a kerr oscillator: From semiclassical \mathcal{PT} symmetry to quantum fluctuations”, *Phys. Rev. A* **103**, 033711 (2021).
- [66] X.-W. Luo, C. Zhang, and S. Du, “Quantum squeezing and sensing with pseudo-anti-parity-time symmetry”, *Phys. Rev. Lett.* **128**, 173602 (2022).
- [67] J. M. P. Nair, D. Mukhopadhyay, and G. S. Agarwal, “Enhanced sensing of weak anharmonicities through coherences in dissipatively coupled anti- \mathcal{PT} symmetric systems”, *Phys. Rev. Lett.* **126**, 180401 (2021).
- [68] M. Aspelmeyer, T. J. Kippenberg, and F. Marquardt, “Cavity optomechanics”, *Rev. Mod. Phys.* **86**, 1391 (2014).
- [69] J. D. Thompson, B. M. Zwickl, A. M. Jayich, F. Marquardt, S. M. Girvin, and J. G. E. Harris, “Strong dispersive coupling of a high-finesse cavity to a micromechanical membrane”, *Nature (London)* **452**, 72 (2008).
- [70] J. C. Sankey, C. Yang, B. M. Zwickl, A. M. Jayich, and J. G. E. Harris, “Strong and tunable nonlinear optomechanical coupling in a low-loss system”, *Nat. Phys.* **6**, 707 (2010).
- [71] M. Karuza, M. Galassi, C. Biancofiore, C. Molinelli, R. Natali, P. Tombesi, G. D. Giuseppe, and D. Vitali, “Tunable linear and quadratic optomechanical coupling for a tilted membrane within an optical cavity: theory and experiment”, *J. Opt.* **15**, 025704 (2012).
- [72] J. Sheng, X. Wei, C. Yang, and H. Wu, “Self-Organized Synchronization of Phonon Lasers”, *Phys. Rev. Lett.* **124**, 053604 (2020).
- [73] P. Z. G. Fonseca, E. B. Aranas, J. Millen, T. S. Monteiro, and P. F. Barker, “Nonlinear dynamics and strong cavity cooling of levitated nanoparticles”, *Phys. Rev. Lett.* **117**, 173602 (2016).
- [74] U. Delić, M. Reisenbauer, D. Grass, N. Kiesel, V. Vuletić, and M. Aspelmeyer, “Cavity cooling of a levitated nanosphere by coherent scattering”, *Phys. Rev. Lett.* **122**, 123602 (2019).
- [75] N. P. Bullier, A. Pontin, and P. F. Barker, “Quadratic optomechanical cooling of a cavity-levitated nanosphere”, *Phys. Rev. Research* **3**, L032022 (2021).
- [76] T. P. Purdy, D. W. C. Brooks, T. Botter, N. Brahms, Z.-Y. Ma, and D. M. Stamper-Kurn, “Tunable cavity optomechanics with ultracold atoms”, *Phys. Rev. Lett.* **105**, 133602 (2010).
- [77] J. T. Hill, “Nonlinear Optics and Wavelength Translation via Cavity-Optomechanics” (Ph.D. thesis, California Institute of Technology, 2013).
- [78] C. Doolin, B. D. Hauer, P. H. Kim, A. J. R. MacDonald, H. Ramp, and J. P. Davis, “Nonlinear optomechanics in the stationary regime”, *Phys. Rev. A* **89**, 053838 (2014).
- [79] G. A. Brawley, M. R. Vanner, P. E. Larsen, S. Schmid, A. Boisen, and W. P. Bowen, “Nonlinear optomechanical measurement of mechanical motion”, *Nat. Commun.* **7**, 10988 (2016).
- [80] H. Kaviani, C. Healey, M. Wu, R. Ghobadi, A. Hryciw, and P. E. Barclay, “Nonlinear optomechanical paddle nanocavities”, *Optica* **2**, 271 (2015).
- [81] T. K. Paraíso, M. Kalaei, L. Zang, H. Pfeifer, F. Marquardt, and O. Painter, “Position-squared coupling in a tunable photonic crystal optomechanical cavity”, *Phys. Rev. X* **5**, 041024 (2015).
- [82] A. Di Virgilio, L. Barsotti, S. Braccini, C. Bradaschia, G. Cella, C. Corda, V. Dattilo, I. Ferrante, F. Fidecaro, I. Fiori, F. Frasconi, A. Gennai, A. Giazotto, P. La Penna, G. Losurdo, E. Majorana, M. Mantovani, A. Pasqualetti, D. Passuello, F. Piergiovanni, A. Porzio, P. Puppo, P. Rapagnani, F. Ricci, S. Solimeno, G. Vajente, and F. Vetrano, “Experimental evidence for an optical spring”, *Phys. Rev. A* **74**, 013813 (2006).
- [83] M. Hossein-Zadeh and K. J. Vahala, “Observation of optical spring effect in a microtoroidal optomechanical resonator”, *Opt. Lett.* **32**, 1611 (2007).
- [84] F. Tian, G. Zhou, Y. Du, F. S. Chau, and J. Deng, “Optical spring effect in nanoelectromechanical systems”, *Appl. Phys. Lett.* **105**, 061115 (2014).

- [85] W. P. Bowen and G. J. Milburn, “Quantum Optomechanics” (CRC Press, Boca Raton, 2015).
- [86] X. Mao, G.-Q. Qin, H. Yang, H. Zhang, M. Wang, and G.-L. Long, “Enhanced sensitivity of optical gyroscope in a mechanical parity-time-symmetric system based on exceptional point”, *New J. Phys.* **22**, 093009 (2020).
- [87] T. Li, W. Wang, and X. Yi, “Enhancing the sensitivity of optomechanical mass sensors with a laser in a squeezed state”, *Phys. Rev. A* **104**, 013521 (2021).
- [88] P. Djorwe, Y. Pennec, and B. Djafari-Rouhani, “Exceptional point enhances sensitivity of optomechanical mass sensors”, *Phys. Rev. Applied* **12**, 024002 (2019).
- [89] Y. Zhi, X.-C. Yu, Q. Gong, L. Yang, and Y.-F. Xiao, “Single Nanoparticle Detection Using Optical Microcavities”, *Adv. Mater.* **29**, 1604920 (2017).
- [90] J.-J. Li and K.-D. Zhu, “All-optical mass sensing with coupled mechanical resonator systems”, *Phys. Rep.* **525**, 223 (2013).
- [91] F. Liu, S. Alaie, Z. C. Leseman, and M. Hossein-Zadeh, “Sub-pg mass sensing and measurement with an optomechanical oscillator”, *Opt. Express* **21**, 19555 (2013).
- [92] Y. He, “Sensitivity of optical mass sensor enhanced by optomechanical coupling”, *Appl. Phys. Lett.* **106**, 121905 (2015).
- [93] W. Yu, W. C. Jiang, Q. Lin, and T. Lu, “Cavity optomechanical spring sensing of single molecules”, *Nat. Commun.* **7**, 12311 (2016).
- [94] Q. Lin, B. He, and M. Xiao, “Mass sensing by detecting the quadrature of a coupled light field”, *Phys. Rev. A* **96**, 043812 (2017).
- [95] S. Liu, B. Liu, J. Wang, T. Sun, and W.-X. Yang, “Realization of a highly sensitive mass sensor in a quadratically coupled optomechanical system”, *Phys. Rev. A* **99**, 033822 (2019).
- [96] M. Sansa, M. Defoort, A. Brenac, M. Hermouet, L. Banniard, A. Fafin, M. Gely, C. Masselon, I. Favero, G. Jourdan, and S. Hentz, “Optomechanical mass spectrometry”, *Nat. Commun.* **11**, 3781 (2020).
- [97] H. Jing, S. K. Özdemir, H. Lü, and F. Nori, “High-order exceptional points in optomechanics”, *Sci. Rep.* **7**, 3386 (2017).
- [98] Y.-L. Liu and Y.-x. Liu, “Energy-localization-enhanced ground-state cooling of a mechanical resonator from room temperature in optomechanics using a gain cavity”, *Phys. Rev. A* **96**, 023812 (2017).
- [99] P. Cao, Y. Li, Y. Peng, C. Qiu, and X. Zhu, “High-order exceptional points in diffusive systems: Robust apt symmetry against perturbation and phase oscillation at apt symmetry breaking”, *ES Energy Environ.* **7**, 48 (2020).
- [100] S. M. Zhang, X. Z. Zhang, L. Jin, and Z. Song, “High-order exceptional points in supersymmetric arrays”, *Phys. Rev. A* **101**, 033820 (2020).
- [101] R. Huang, S. K. Özdemir, J.-Q. Liao, F. Minganti, L.-M. Kuang, F. Nori, and H. Jing, “Exceptional Photon Blockade: Engineering Photon Blockade with Chiral Exceptional Points”, *Laser Photonics Rev.* **16**, 2100430 (2022).
- [102] E. J. Bergholtz, J. C. Budich, and F. K. Kunst, “Exceptional topology of non-hermitian systems”, *Rev. Mod. Phys.* **93**, 015005 (2021).
- [103] H. C. Wu, L. Jin, Z. Song, “Topology of an anti-parity-time symmetric non-Hermitian Su-Schrieffer-Heeger model”, *Phys. Rev. B* **103**, 235110 (2021).
- [104] Z.-H. Xu, X. Xia, and S. Chen, “Exact mobility edges and topological phase transition in two-dimensional non-Hermitian quasicrystals”, *Sci. China Phys. Mech. Astron.* **65**, 227211 (2022).
- [105] J.-S. Tang, W. Nie, L. Tang, M. Chen, X. Su, Y. Lu, F. Nori, and K. Xia, “Nonreciprocal Single-Photon Band Structure”, *Phys. Rev. Lett.* **128**, 203602 (2022).
- [106] Y. Tang, C. Liang, X. Wen, W. Li, A.-N. Xu, and Y.-C. Liu, “ \mathcal{PT} -Symmetric Feedback Induced Linewidth Narrowing”, *Phys. Rev. Lett.* **130**, 193602 (2023).
- [107] J. Leuthold, C. Koos, and W. Freude, “Nonlinear silicon photonics”, *Nature Photon.* **4**, 535 (2010).